The electrospray cone-jet mode for weakly viscoelastic liquids

S. Blanco-Trejo, M. A. Herrada, and A. M. Gañán-Calvo

Escuela Técnica Superior de Ingenieros, Universidad de Sevilla,

Avda. de los Descubrimientos s/n, E-41092-Sevilla, Spain

José M. Montanero

Departmento de Ingeniería Mecánica,

Energética y de los Materiales and

Instituto de Computación Científica Avanzada (ICCAEx),

Universidad de Extremadura, Avda. de Elvas s/n, E-06071 Badajoz, Spain

(Dated: October 14, 2019)

Abstract

We study theoretically the influence of viscoelasticity on the steady cone-jet mode of electrospray for small stress relaxation times. For this purpose, we numerically integrate the leaky-dielectric model together with the Oldroyd-B constitutive relationship, and calculate both the base flow and linear eigenmodes characterizing its stability as a function of the governing parameters. We describe the effect of the polymeric stresses on both the cone-jet mode and the minimum flow rate stability limit. There are considerable differences between the Newtonian and viscoelastic electrospray realizations even for relatively small stress relaxation times due to the intense extensional deformation suffered by the fluid particles in the cone-jet transition region The axial polymeric stress shrinks the liquid meniscus and stabilizes it by pushing the fluid particle in the cone-to-jet transition region.

I. INTRODUCTION

Electrospinning of polymer solutions is a widely used technique for the fabrication of polymer fibers with diameters ranging from tens of microns down to a few nanometers [1]. Several medical areas, like tissue engineering or drug delivery [2], benefit from this technique. Electrospinning produces nanofibers with specific photonic, electronic, magnetic and photocatalytic properties demanded in a number of technical fields. Areas like textile and filter applications have benefited from electrospinning as well [3].

Despite its wide applicability, the liquid ejection in electrospinning is far from being fully understood. Most theoretical studies are based on the 1D (slenderness) approximation for the axial momentum equation [4, 5], which allows for a simple description of the balance between the forces driving and opposing the liquid motion. Carroll and Joo [6] conducted a "hybrid" local-global linear stability analysis for low-conductivity viscoelastic liquids in which the axially non-uniform base flow was numerically calculated from the 1D model, and was perturbed with normal modes. The analysis was subsequently extended to highly-conducting polymer solutions [7]. If the stress relaxation time is large enough for the polymer coil-stretch transition to take place in the unperturbed state, the axisymmetric mode drastically stabilizes. This mode has a capillary and electrical origin for low and high conductivities, respectively. Dharmansh and Chokshi [8] conducted the global linear stability analysis of a low-conductivity Newtonian jet in the framework of the 1D model too. They showed the stabilizing effect of the jet thinning, and attributed that effect to both the variation of the surface charge density and the extensional deformation rate in the base flow. Similar conclusions were obtained when rheological effects were considered [9]. To the best of our knowledge, there is neither analytical nor numerical 2D (axisymmetric) solution of the cone-jet mode in electrospinning. The calculation of the scaling laws for the jet diameter and current intensity commonly applied in electrospray of Newtonian liquids [10] does not have its counterpart in electrospinning either.

Weakly viscoelastic polymer solutions with quasi-monodisperse molecular weight distributions exhibit a constant viscosity μ_0 over a wide interval of shear rates (shear thinning can be neglected) and elastic properties that can be approximately quantified by a single characteristic relaxation time $\widetilde{\lambda}_s$ [11]. The Oldroyd-B model [12] is one of the simplest approximations for calculating the total extra stress tensor of this type of non-Newtonian

liquids because it assumes a linear relationship between the polymer stress and conformation tensor, and a linear relaxation law for the latter. This simplicity, and the fact that it can be derived from kinetic theory for a fluid filled with elastic beads and spring dumbbells [13], has conferred remarkable popularity upon this model [14]. One of its fundamental limitations is the fact that it does not take into account the finite extensibility of the polymers, and, therefore, it cannot describe phenomena like the appearance of blistering in capillary thinning [15, 16].

The Taylor-Melcher leaky-dielectric model [17, 18] has been successfully applied to the description of the steady cone-jet mode of electrospray [19–22]. In this approximation, the net free charge accumulates within a very thin Debye layer formed at the free surface, which collects free charge from the bulk at a rate given by a constant electrical conductivity. A natural question is whether this last condition still holds under the anisotropic conditions arising in electrospray with polymer solutions. In this case, the electrical conductivity probably becomes a non-uniform tensorial quantity related to the local value of the polymer conformation tensor, which accounts for the expected difference between the electrical resistivity along the radial and axial directions of electrospray. Given the absence of experimental measurements to support this or any other correlation, researchers have simply extended the Newtonian leaky-dielectric model to the viscoelastic case by replacing the Newtonian constitutive relationship by the Oldroyd-B or FENE-P model [4, 5, 9].

The cone-jet mode of electrospray is intrinsically unstable because the breakup of the emitted jet into drops is always an energetically favorable process. The question is whether one can identify a fluid domain portion, which includes an ejected thread long as compared to its diameter, where the flow remains essentially steady. The most accurate approach to address this question is the global linear stability analysis [23]. In this analysis, one asks the system whether small-amplitude perturbations introduced at a given instant in the considered fluid domain decay asymptotically on time in the Eulerian frame of reference. For this purpose, one firstly calculates the axisymmetric stationary solution $U_0(r,z)$ framed within the considered fluid domain, and then obtains the global modes

$$\{\delta U^{(k)}(r,z)\ \exp[i(m\theta-\omega_m^{(k)}t)]\}\quad (k=1,2,\ldots,N) \tag{1}$$

of that base flow. Here, the symbol U represents any hydrodynamic quantity, r and z are the cylindrical coordinates (z is the symmetry axis), and $\omega_m^{(k)}=\omega_{mr}^{(k)}+i\omega_{mi}^{(k)}$ is the eigenfrequency

characterizing the temporal evolution of the linear mode with azimuthal number m. If all the growth factors $\{\omega_{mi}^{(k)}\}$ are negative, any perturbation decays for long times, and the base flow is asymptotically stable [23]. The linear superposition of decaying modes excited by a given perturbation may lead to the short-term growth of that perturbation. In some cases, this effect can destabilize an asymptotically stable flow [24], like occurs in gaseous flow focusing [25]. However, this possibility has not been observed in Newtonian electrospray, where the minimum flow rates predicted by the global stability analysis agree fairly well with the experimental values [21]. Therefore, it is reasonable to identify asymptotic stability with linear stability in the weakly viscoelastic case too.

This work can be regarded as a first attempt to extend the 2D numerical analyses of electrospray for Newtonian liquids [19–22] to weakly viscoelastic fluids. We will study how elasticity influences the flow pattern, meniscus shape, superficial electric field, and both driving and resistant forces arising in the cone-jet mode of electrospray. We will examine the effect of elasticity on the linear stability of this mode under axisymmetric $m = 0$ perturbations.

II. THE CONE-JET MODE OF ELECTROSPRAY

To gain insight into the time and spatial scales characterizing the weakly viscoelastic electrospray, we here borrow some well-established results from the Newtonian case. The parameters which essentially characterize the steady cone-jet mode of electrospray are the issued flow rate Q and both the liquid and outer environment properties. The properties of a leaky-dielectric Oldroyd-B liquid are the density ρ, (zero-shear) viscosity μ_0, stress (polymer) relaxation time $\widetilde{\lambda}_s$, retardation time $\widetilde{\lambda}_r$, surface tension γ, electrical permittivity ε_i, and electrical conductivity K. As can be seen, we assume that the presence of macromolecules does not significantly alter the isotropic character of electric conduction. This approximation applies to viscoelastic solutions whose molecular composition leads to significant mechanical anisotropy but quasi-isotropic ionic diffusion. If the outer environment is either vacuum or a gas, its dynamical effect on the liquid can be neglected, and the only parameter characterizing its electrical influence is its permittivity ε_o.

There is a narrow interval of the applied voltage V within which the steady cone-jet mode can be established. For this reason, and as a first approximation, one does not regard this

quantity as a governing parameter. In the steady cone-jet mode, conduction gives way to dominant charge convection over the liquid surface within the so-called cone-jet transition region [10]. Forces driving and opposing the fluid motion emerge in this critical region, whose size is typically much smaller than that of the electrospray device. Due to the local character of electrospray, the device geometrical features and associated lengths play a secondary role in this phenomenon.

Under the above conditions, one defines the characteristic radial length $d_o = [\gamma\varepsilon_o^2/(\rho K^2)]^{1/3}$, axial velocity $v_o = [\gamma K/(\rho\varepsilon_o)]^{1/3}$, electric relaxation time $t_o = \varepsilon_i/K$, electric field $E_o = (\gamma^2\rho K^2/\varepsilon_o^5)^{1/6}$ and current intensity $I_o = \gamma\rho^{-1/2}\varepsilon_o^{1/2}$ in terms of the electrodynamic properties of the fluids exclusively. Five dimensionless parameters can be formed with the first three characteristic quantities introduced above and the liquid density and viscosity: the relative permittivity $\beta = v_o t_o/d_o = \varepsilon_i/\varepsilon_o$, the electrohydrodynamic Reynolds number $\delta_\mu = \rho v_o d_o/\mu_0 = [\gamma^2\rho\varepsilon_o/(\mu^3 K)]^{1/3}$, the dimensionless stress relaxation time $\lambda_s = \widetilde{\lambda}_s/t_o = \widetilde{\lambda}_s/(\beta d_o/v_o)$, the dimensionless retardation time $\lambda_r = \widetilde{\lambda}_r/\widetilde{\lambda}_s$, and the relative flow rate $Q_r = Q/Q_o$, where $Q_o = v_o d_o^2 = \gamma\varepsilon_o/(\rho K)$.

The characteristic axial length L of the cone-jet transition region in Newtonian electrospray can be estimated as $L \sim d_o Q_r$ [10], while the liquid velocity in that region scales as v_o. Therefore, the residence time t_r in the cone-jet transition region scales as $t_r \sim L/v_o \sim d_o Q_r/v_o$. The fluid particle accelerates from a negligible velocity up to the jet speed $v_j \sim v_o$ within the cone-jet transition region. Therefore, the axial strain rate $\dot{\varepsilon}$ in the critical region scales as $\dot{\varepsilon} \sim v_j/L \sim v_0/(d_0 Q_r)$ [21].

The minimum flow rate stability limit is probably the most relevant parameter region at the practical level, because relatively monodisperse streams of droplets are produced with their minimum size in that region. The Buckingham π theorem [26] shows that any dimensionless number describing the steady cone-jet mode behavior must be a function of the above-introduced governing parameters. In particular, $Q_{r\min} = Q_{r\min}(\beta, \delta_\mu, \lambda_s, \lambda_r)$, where $Q_{r\min} = Q_{\min}/Q_o$ and $Q_{\min}$ is the minimum flow rate. In the Newtonian inviscid (polarity-dominated) limit $\beta\delta_\mu \gg 1$, a simple scaling analysis shows that $Q_{r\min} \sim \beta$ [27]. Then, the residence time in the cone-jet transition region becomes $t_r \sim d_o\beta/v_o = t_o$. Therefore, and under the conditions mentioned above, the dimensionless stress relaxation time $\lambda_s = \widetilde{\lambda}_s/t_o$ can be interpreted as the Deborah number, i.e., the stress relaxation time $\widetilde{\lambda}_s$ measured in terms of the residence time t_r in the critical cone-jet transition region. In addition, the

axial strain rate in that region scales as $\dot{\varepsilon} \sim v_0/(d_0\beta) = t_o^{-1}$, and, therefore, λ_s can also be regarded as the Weissenberg number, i.e., the strain rate times the stress relaxation time.

When the radial and/or axial dimension of the cone-jet transition region are commensurate with the Taylor meniscus size, the latter may affect some features of the cone-jet mode. In this case, one defines the diameter ratio $\Lambda = 2R_i/d_o = 2[\rho K^2 R_i^3/(\gamma\varepsilon_o^2)]^{1/3}$, where R_i is the radius of the triple contact line anchored at the feeding capillary end. For $\Lambda \lesssim 10^2$, the cone-jet mode stability can be influenced by the feeding capillary size [28]. This may occur, for instance, in the cone-jet mode of nanoelectrospray [29, 30].

III. THE LEAKY-DIELECTRIC OLDROYD-B MODEL

In this section, we present the equations defining the leaky-dielectric Oldroyd-B model and describe the numerical method used to calculate both the base flows and their linear stability. In this work, we restrict ourselves to the analysis of the $m = 0$ mode, and, therefore, the model is axisymmetric. Both the model and the numerical method are the natural extensions of those recently used to study the cone-jet mode of Newtonian electrospray [21].

Figure 1 represents the geometrical and electrical configurations considered in the simulations. The red rectangle corresponds to the computational domain. A cylindrical capillary is held at a constant voltage V. The capillary is brought face to face up close to a planar grounded electrode located at a distance H'. A liquid is injected through the capillary at a constant flow rate Q. The flow is fully developed inside the capillary, so that there is a parabolic Hagen-Poiseuille velocity profile upstream at a distance L_n from the capillary's exit. The triple contact line anchors at a distance R_i from the capillary axis. The ambient medium is a perfect dielectric gas whose dynamic effects are neglected. To analyze the global stability of the jetting regime, we set a boundary in the downstream direction and apply outflow (passive) boundary conditions at that cutoff. The gravitational Bond number takes sufficiently small values for the gravity effects to be inconsequential. In what follows, all the quantities are made dimensionless with the triple contact line radius R_i, the liquid density ρ, the surface tension γ, and the applied voltage V, which yields the characteristic time, velocity, pressure and electric field scales $t_c = (\rho R_i^3/\gamma)^{1/2}$, $v_c = R_i/t_c$, $p_c = \gamma/R_i$ and $E_c = V/R_i$, respectively. It must be noted that theses quantities differ from those defined in Sec. II to describe the critical cone-jet transition region because the present model considers

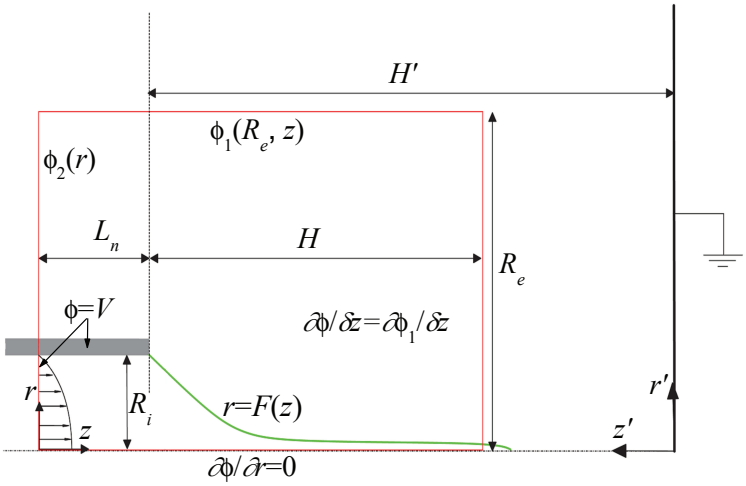

FIG. 1. (Color online) Sketch of the problem's formulation. The rectangle (red online) denotes the limits of the computational domain.

the entire fluid configuration.

The (dimensionless) velocity $\mathbf{v}(\mathbf{r},t) = u(r,z,t)\mathbf{e_r} + w(r,z,t)\mathbf{e_z}$ and reduced pressure $p(r,z,t)$ fields are calculated from the continuity and momentum equations

$$\boldsymbol{\nabla}\cdot\mathbf{v} = 0, \tag{2}$$

$$\frac{\partial \mathbf{v}}{\partial t} + \mathbf{v}\cdot\boldsymbol{\nabla}\mathbf{v} = -\boldsymbol{\nabla}p + \boldsymbol{\nabla}\cdot\mathbf{T}. \tag{3}$$

The extra stress tensor $\mathbf{T}$ in the Oldroyd-B model can be seen as the sum of the solvent contribution and that due to the presence of polymers, which is given by the Maxwell model [31]. The result is

$$(1+\lambda_s^*\mathsf{G})\,\mathbf{T} = \mathrm{Oh}_0(1+\lambda_r^*\mathsf{G})[\boldsymbol{\nabla}\mathbf{v} + (\boldsymbol{\nabla}\mathbf{v})^T]\,, \tag{4}$$

where $\lambda_s^* = \widetilde{\lambda}_s/t_c$ is the stress relaxation time defined in terms of the capillary time [32], $\mathsf{G}[\mathsf{A}]$ the upper convected derivative operator, $\mathrm{Oh}_0 = \mu_0(\rho R\sigma)^{-1/2}$ the Ohnesorge number, $\lambda_r^* = \lambda_s^*\mu^{(s)}/\mu_0$ the dimensionless retardation time, and $\mu^{(s)}$ the solvent viscosity. In most viscoelastic liquids, the solution viscosity considerably increases when the polymer is added to the solvent. For this reason, we will assume that $\mu^{(s)} \ll \mu_0$ and, therefore, $\lambda_r^* \simeq 0$.

In the leaky-dielectric model, the bulk net free charge is assumed to be negligible, and, therefore, the electric potentials ϕ^i and ϕ^o in both the inner (liquid) and outer (gas) domains obey the Laplace equation

$$\phi^{i,o}_{zz} + \phi^{i,o}_{rr} + \phi^{i,o}_{r}/r = 0. \tag{5}$$

The subscripts r and z here and henceforth denote the partial derivatives with respect to the corresponding spatial variables.

The free surface location is defined by the equation $r = F(z,t)$. The boundary conditions at that surface are:

$$\frac{\partial F}{\partial t} + F_z w - u = 0, \tag{6}$$

$$p + \frac{F F_{zz} - 1 - F_z^2}{F(1+F_z^2)^{3/2}} + \mathbf{n}\cdot\mathbf{T}\cdot\mathbf{n} = \frac{\chi}{2}\left[(E_n^o)^2 - \beta(E_n^i)^2\right] + \chi\frac{\beta-1}{2}(E_t)^2, \tag{7}$$

$$\mathbf{t}\cdot\mathbf{T}\cdot\mathbf{n} = \chi\sigma E_t, \tag{8}$$

where $\mathbf{n}$ is the unit outward normal vector, $\chi = \varepsilon_o V^2/(R_i\gamma)$ is the electric Bond number, $\mathbf{E}^i$ and $\mathbf{E}^o$ stand for the inner and outer electric field, respectively, $\mathbf{t}$ is the unit vector tangential to the free surface meridians, and σ the superficial charge density. Equation (6) is the kinematic compatibility condition, while Eqs. (7) and (8) express the balance of normal and tangential stresses on the two sides of the free surface, respectively. The right-hand sides of these equations are the Maxwell stresses resulting from both the accumulation of free electric charges at the interface and the jump of permittivity across that surface.

The electric field at the free surface and the surface charge density are calculated as

$$E_n^i = \frac{F_z\phi_z^i - \phi_r^i}{\sqrt{1+F_z^2}}, \quad E_n^o = \frac{F_z\phi_z^o - \phi_r^o}{\sqrt{1+F_z^2}}, \tag{9}$$

$$E_t = \frac{-F_z\phi_r^o + \phi_z^o}{\sqrt{1+F_z^2}} = \frac{-F_z\phi_r^i + \phi_z^i}{\sqrt{1+F_z^2}}, \tag{10}$$

$$\sigma = \chi(E_n^o - \beta E_n^i). \tag{11}$$

It must be noted that the continuity of the electric potential across the free surface, $\phi^i = \phi^o$, has been considered in Eq. (10).

The free surface equations are completed by imposing the surface charge conservation at $r = F(z,t)$,

$$\frac{\partial\sigma}{\partial t} + \boldsymbol{\nabla_s}\cdot(\sigma\mathbf{v}) = \chi\alpha E_n^i, \tag{12}$$

where $\boldsymbol{\nabla_s}$ is the tangential intrinsic gradient along the free surface, and $\alpha = K\left[\rho R_i^3/(\gamma\varepsilon_o^2)\right]^{1/2}$ is the dimensionless electrical conductivity.

As mentioned above, the Hagen-Poiseuille velocity profile is prescribed at the entrance of the liquid domain $z = 0$:

$$u = 0, \quad w = 2\mathcal{Q}(1-r^2), \tag{13}$$

where $\mathcal{Q} = Q/(\pi R_i^2 v_c)$. At the capillary wall, we fix the electric potential and impose no-slip boundary conditions, i.e.,

$$\phi^i = \phi^e = 1 \quad \text{and} \quad u = w = 0. \tag{14}$$

The triple contact line is anchored at the end of the capillary:

$$F = 1 \quad \text{at} \quad z = L_n. \tag{15}$$

The standard regularity conditions

$$\phi_r^i = u = w_r = 0 \tag{16}$$

are prescribed on the symmetry axis, and the outflow conditions

$$u_z = w_z = F_z = \sigma_z = 0 \tag{17}$$

are considered at the right-hand end $z_e = H + L_n$ of the computational domain.

The analytical solution for the far-field electric potential [33],

$$\phi_1(r', z') = \frac{-K_v}{\log(4H')} \log\left\{ \frac{[r'^2 + (1 - z')^2]^{1/2} + (1 - z')}{[r'^2 + (1 + z')^2]^{1/2} + (1 + z')} \right\}, \tag{18}$$

is imposed at the boundary $r = R_e$. Here, r' and z' are cylindrical coordinates with origin at the intersection between the symmetry axis and the grounded planar electrode (see Fig. 1), while K_v is a dimensionless constant which depends on H'. A logarithmic drop of voltage

$$\phi_2 = 1 - [1 - \phi_1(r_e, z_e^{'})] \log r / \log R_e, \quad z_e^{'} \equiv H' + L_n, \tag{19}$$

is applied at the boundary $z = 0$ and $1 < r < R_e$. Finally, the condition

$$\phi_z = (\phi_1)_z \tag{20}$$

is imposed at the right-hand end $z = z_e$ of both the liquid and gas computational domains.

The base flow of the steady cone-jet mode is calculated as the solution of the above equations eliminating the partial derivatives of the unknowns with respect to time. The simulation allows one to obtain the total current intensity I as the sum of the contributions due to the bulk conduction I_b and surface convection I_s. These contributions can be calculated at any axial position z along the cone-jet as

$$I_b(z) = 2\pi\alpha\chi \int_0^{F(z)} E_z^i(r, z)\, r\, dr, \quad I_s(z) = 2\pi F(z)\sigma(z)v_s(z), \tag{21}$$

where E_z^i is the axial component of the inner electric field, and $v_s(z)$ is the free surface velocity. Both the free surface position and current intensity have been calculated and compared with experimental data for 1-octanol, showing good agreement [20].

To calculate the linear axisymmetric global modes, one assumes the temporal dependence

$$U(r,z;t) = U_0(r,z) + \epsilon \delta U^{(k)}(r,z)\, e^{-i\omega^{(k)}t} \quad (\epsilon \ll 1). \tag{22}$$

Here, $U(r,z;t)$ represents any hydrodynamic quantity, $U_0(r,z)$ and $\delta U^{(k)}(r,z)$ stand for the base (steady) solution and the spatial dependence of the kth eigenmode, respectively, while $\omega^{(k)} = \omega_r^{(k)} + i\omega_i^{(k)}$ is the eigenfrequency. Both the eigenfrequencies and the corresponding eigenmodes are calculated as a function of the governing parameters. The dominant eigenmode is that with the largest growth factor. If that growth factor is positive, the base flow is asymptotically unstable [23]. We restrict our study to the dominant mode, whose eigenfrequency is $\omega = \omega_r + i\omega_i$.

The governing equations are formulated in terms of the dimensionless numbers $\{\mathrm{Oh}_0,\, \lambda_s^*,\, \lambda_r^*,\, \beta,\, \chi,\, \alpha,\, \mathcal{Q}\}$ and those characterizing the rest of boundary conditions. The parameters of the first set can be combined to get the dimensionless numbers $\{\beta,\, \delta_\mu,\, \lambda_s,\, \lambda_r,\, Q_r\}$ introduced in Sec. II; specifically,

$$\delta_\mu = \alpha^{-1/3}\mathrm{Oh}_0^{1/2}, \quad \lambda_s = \alpha\beta^{-1}\lambda_s^*, \quad \lambda_r = \alpha\beta^{-1}\lambda_r^*, \quad Q_r = \pi\,\alpha\,\mathcal{Q}. \tag{23}$$

The dimensionless conductivity $\alpha = \beta t_c/t_o$ takes values much greater than unity because the electric relaxation time t_o is much smaller than the capillary one t_c. This implies that $\lambda_s \gg \lambda_s^*$. It must be noted that the effect of viscoelasticity in electrospray is better quantified by the dimensionless relaxation time λ_s, because it measures the time for the polymer to relax to its coiling state in terms of the residence time t_o in the stretching region.

Most polymeric solutions exhibit zero-shear viscosities much larger than those of their corresponding solvents. For this reason, we will take $\lambda_r^* \simeq 0$ in our calculations. As explained in Sec. II, the influence of the geometrical parameters can be neglected if one takes into account both the locality of the jet emission phenomenon and the secondary role of the electrical potential. In particular, the results are not expected to depend on the length H of the computational domain for sufficiently large values of this parameter. We set $H = 12$ and verified that neither the base flow nor its eigenmodes significantly varied when that parameter was considerably increased. In addition, the length of the feeding capillary was

$L_n = 1.5$, the distance between the two electrodes was $H' = 20$, and the radial distance of the outer boundary from the symmetry axis was $R_e = 6$.

We use the numerical method proposed by Herrada and Montanero [34] to solve the model described in this section. The application of that model to the electrospray configuration, as well as its validation for Newtonian liquids, have been recently described by Ponce-Torres et al. [21]. The inclusion of the polymeric stresses does not modify any substantial aspect of the numerical method. We refer interested readers to that work for more details of the procedure.

The addition of elastic stresses limits the numerical stability of the algorithm used to find the base flow solution. As mentioned in Sec. II, the strain rate in the cone-jet transition region of Newtonian electrospray scales as $\dot{\varepsilon} \sim\sim v_0/(d_0 Q_r)$. This means that the polymeric stress increases in that critical region as the flow rate decreases. This sets an upper limit to the stress relaxation time for a fixed flow rate, and a lower limit for the flow rate for a fixed stress relaxation time. On the other hand, the retardation time somehow quantifies the energy dissipation due to the solvent viscosity. Numerical instabilities are damped out by the solvent viscous stresses, which sets a lower limit for the retardation time too.

IV. RESULTS

In this section, we study the effects of viscoelasticity on the electrospray cone-jet mode of 1-octanol ($\rho = 827$ kg/m^3, $\mu = 7.20$ mPa s, $\gamma = 23.5$ mN/m, $K = 9.0 \times 10^{-7}$, $\beta = 10$, $\delta_\mu = 2.29$), whose numerical simulation has been validated experimentally [20, 21]. This liquid corresponds to a moderately low-viscosity (polarity-dominated) case. The feeding capillary radius $R_i = 550$ μm is sufficiently large for the jet emission to be regarded as a local phenomenon [21]. All the simulations are conducted for the electric Bond number $\chi = 7.92$. In Figs. 2–7, we examine the effect of viscoelasticity by considering the stress relaxation time $\widetilde{\lambda}_s = 261$ μs, which is sufficiently large to produce noticeable effects, and small enough for the liquid to be considered as a weakly viscoelastic solution [35]. We take the retardation time value $\widetilde{\lambda}_r = 24.2$ μs, which is much smaller than $\widetilde{\lambda}_s$ but sufficiently large to damp out numerical instabilities. The influence of viscoelasticity on the minimum flow rate stability limit is studied in Fig. 8 for different stress relaxation times λ_s while keeping constant the ratio λ_r/λ_s, i.e. for a fixed solution viscosity.

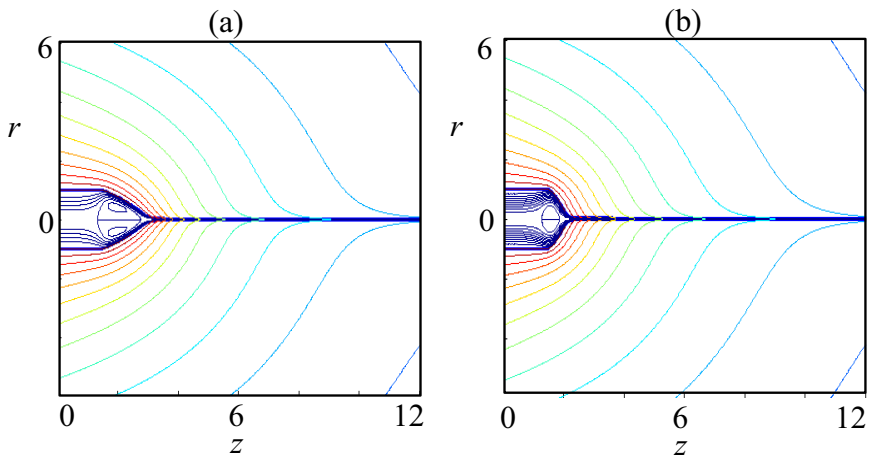

FIG. 2. (Color online) Base flows for $\beta = 10$, $\delta_\mu = 2.29$, $\chi = 7.92$, $Q_r = 7.72$, $\lambda_r = 0.0926\lambda_s$, and $\lambda_s = 0$ (a) and 2.656 ($\lambda_s^* = 0.108$) (b). The lines in the inner and outer domains correspond to the streamlines and equipotential lines, respectively.

There is a considerable difference between the flow patterns of the Newtonian and viscoelastic cone-jet modes (Fig. 2). When viscoelasticity is added to the electrosprayed liquid, the meniscus shrinks significantly. For sufficiently small flow rates, a recirculation cell appears in the cone. As can be observed, that cell also shrinks in the non-Newtonian case.

Figure 3 shows the real and imaginary parts of the eigenvalue responsible for the instability of the base flow as a function of the flow rate Q_r. In the Newtonian case, there is an interval of flow rates for which the growth rates are negative, which means that the system is asymptotically stable in that interval. The maximum flow rate is roughly ten times the minimum one. The loss of stability at the minimum and maximum flow rates is caused by the same eigenmode. The perturbation responsible for instability grows in amplitude while oscillating with a frequency of the order of the capillary time. We do not observe any bifurcation of the base flow when the numerical solution crosses the stability limits. The lowest flow rate explored for the non-Newtonian liquid was limited by numerical instabilities, as explained in Sec. III. For this reason, the minimum flow rate stability limit could not be reached in this case. The dominant eigenmode in the viscoelastic case changes for $Q_r \simeq 10$, which explains the jump of the oscillation frequency at that flow rate. There is little influence of viscoelasticity on both the maximum flow rate and the oscillation frequency of the mode responsible for the instability.

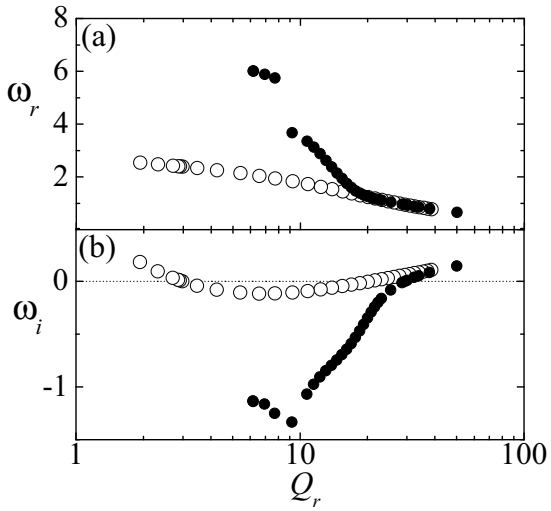

FIG. 3. Real (a) and imaginary (b) part of the eigenvalue responsible for instability as a function of Q_r. The results were calculated for $\beta = 10$, $\delta_\mu = 2.29$, $\chi = 7.92$, $\lambda_r = 0.0926\lambda_s$ and $\lambda_s = 0$ (open symbols) and $\lambda_s = 2.656$ ($\lambda_s^* = 0.108$) (solid symbols).

Fluid particles undergo an intense extensional flow when crossing the cone-jet transition region, where the velocity increases from very small values up to the jet speed. This extensional flow stretches the polymers dissolved in the liquid, which tend to relax to their coiling state on a time scale given by λ_s^*. If this characteristic time is sufficiently large as compared to the axial strain rate, then the stretch-to-coil transition is prevented, and polymers keep on stretching over the cone-jet region. In an uniaxial extensional flow, this occurs for $\dot{\varepsilon}\lambda_s^* > 1/2$. In order to examine this aspect of the problem, we have measured the strain rate $\dot{\varepsilon}$ and both the solvent $T_{zz}^{(s)} = \mathrm{Oh}_s\, \partial w/\partial z$ ($\mathrm{Oh}_s = \mu_s(\rho R\gamma)^{-1/2}$) and polymeric $T_{zz}^{(p)} = T_{zz} - T_{zz}^{(s)}$ contributions to the extra stress tensor along the symmetry axis. Figure 4 shows the results for the case considered in this section. As can be seen, $\dot{\varepsilon}\lambda_s^* > 1/2$ in the cone-jet transition region, which makes the polymer stress sharply increase in that region. For $z \gtrsim 2.6$, the strain rate falls below that critical value mentioned above, and both $T_{zz}^{(p)}$ and $T_{rz}^{(p)}$ decay exponentially. As can be observed, $T_{rz}^{(p)}$ takes relatively small but non-negligible values. The existence of a noticeable off-diagonal stress component of the polymeric stress tensor has also been observed in the later stages of Oldroyd-B filament thinning [36]. The contribution of the solvent viscous stress is hardly noticeable due to the smallness of the retardation time.

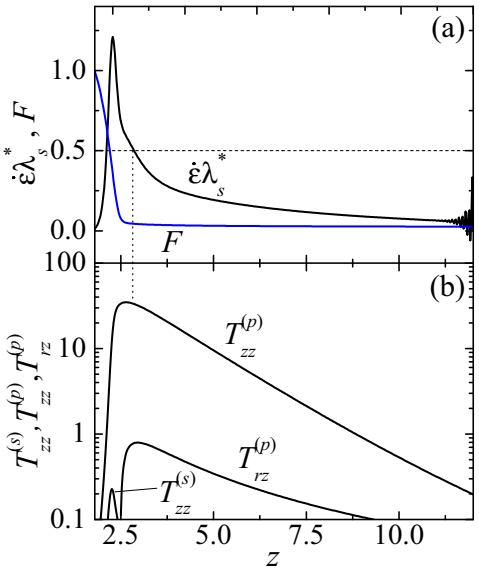

FIG. 4. (Color online) (a) Free surface position F and strain rate $\dot{\varepsilon}$ as a function of the axial position z. (b) Components $T_{zz}^{(p)}$ and $T_{rz}^{(p)}$ of the polymeric stress tensor and solvent contribution $T_{zz}^{(s)}$ as a function of the axial position z. The results were calculated for $\beta = 10$, $\delta_\mu = 2.29$, $\chi = 7.92$, $Q_r = 7.72$, $\lambda_r = 0.0926\lambda_s$ and $\lambda_s = 2.656$ ($\lambda_s^* = 0.108$).

Figure 5 compares the tangential and normal components of the inner and outer electric fields at the free surface for the Newtonian liquid and its viscoelastic counterpart. In both cases, E_n^o is around three times larger than βE_n^i in the cone-jet transition region, and, therefore, one can conclude that the superficial charge is not fully relaxed to its local electrostatic value within that region. The outer normal component E_n^o of the electric field in the Newtonian cone-jet transition region takes values significantly larger than those of the viscoelastic case, which indicates that the energy transmitted by the dominant shear electric stress to the liquid is larger in the absence of elasticity. This is linked to the more stretched shape taken by the Newtonian liquid meniscus. The component E_n^o reaches similar values downstream, which means that the superficial charge density transported by the viscoelastic jet is essentially the same as that convected by the Newtonian one.

In the 1D (slender) approximation, the momentum equation in the z-direction becomes

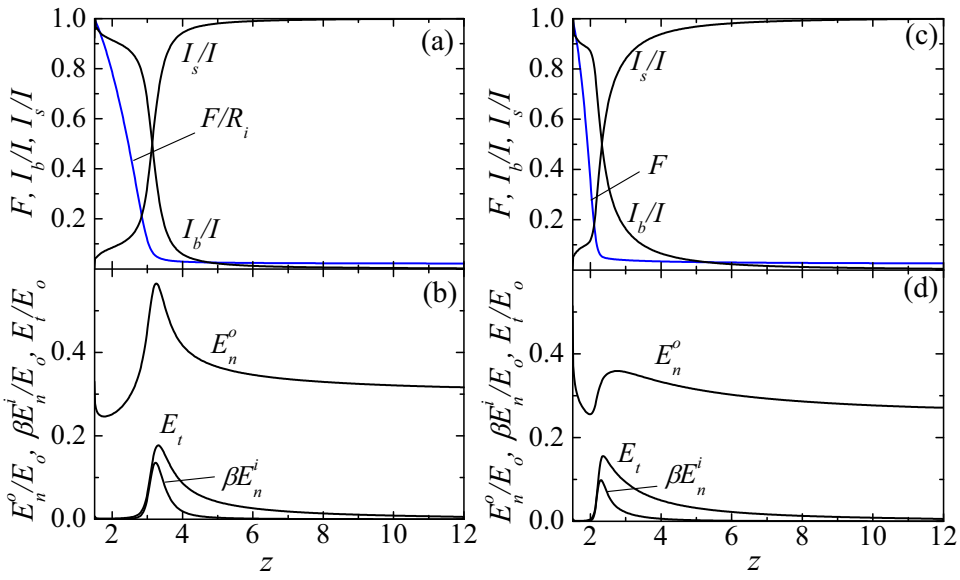

FIG. 5. (Color online) Free surface position F, bulk current intensity I_b and surface current intensity I_s as a function of the axial position z [(a) and (c)]. Tangential E_t and normal components E_n^i and E_n^o of the inner and outer electric fields at the free surface [(b) and (d)]. The results were calculated for $\beta = 10$, $\delta_\mu = 2.29$, $\chi = 7.92$, $Q_r = 7.72$, $\lambda_r = 0.0926\lambda_s$ and $\lambda_s = 0$ (left) and 2.656 ($\lambda_s^* = 0.108$) (right).

[4]:

$$\underbrace{\frac{\chi}{2}\left[(E_n^o)^2 - \beta(E_n^i)^2\right]_z}_{\text{I}} + \underbrace{\chi\frac{\beta-1}{2}\left[(E^t)^2\right]_z}_{\text{II}} + \underbrace{\frac{2\sigma E_t}{F}}_{\text{III}} =$$
$$\underbrace{\left(\frac{1}{F}\right)_z}_{\text{IV}} + \underbrace{\left(\frac{\mathcal{Q}^2}{2F^4}\right)_z}_{\text{V}} + \underbrace{\frac{6\text{Oh}_s\mathcal{Q}}{F^2}\left(\frac{F_z}{F}\right)_z}_{\text{VI}} + \underbrace{\frac{1}{F^2}\left[F^2\left(T_{rr}^{(p)} - T_{zz}^{(p)}\right)\right]_z}_{\text{VII}}. \tag{24}$$

The terms of Eq. (24) have been grouped into electric (left-hand side) and hydrodynamic (right-hand side) forces. The addends I, II and III are generally referred to as the electrostatic, polarization, and electric tangential forces per unit volume, respectively [10]. The terms IV, V, VI and VII correspond to surface tension, inertia, solvent viscosity, and polymeric stress, respectively.

Figure 6 shows the values taken by all the terms of the 1D model (24) as a function of the axial position z. The electric tangential force (III) is the main driving force and acts

not only in the jet emission region but also along the ejected liquid thread. As mentioned above, this force takes considerably larger values in the Newtonian case. The electrostatic suction (I) supplies much less energy, but it plays a relevant role in shaping the cone-jet transition region to produce the liquid ejection. It hinders the flow behind the cone-jet transition region only in the absence of viscoelasticity. Finally, the polarization force pushes the fluid in front of the cone-jet transition region, while opposes the liquid ejection behind that point in the two cases. Most of the work done by the electric field on the Newtonian liquid converts into kinetic energy. Polymers pull from the liquid while stretching in the meniscus apex, and exert a resistant force throughout the jet as they relax to their coiling state. The pulling exerted by the dissolved polymers increases the liquid acceleration, which flattens the meniscus. For this reason, the surface tension constitutes the main energy sink in the viscoelastic cone-jet transition region, and the 1D approximation provides less accurate predictions in that region [see panels (c)]. In fact, this model does not even contemplate the off-diagonal polymeric stress $T_{rz}^{(p)}$, which takes smaller but non-negligible values as compared to those of $T_{zz}^{(p)}$ (Fig. 4). The fact that the maximum of |VII| exceeds the maximum of III reveals the importance of the polymeric axial stress in this flow, despite the smallness of the stress relaxation time.

Figure 7 shows the diameter d_{out} at the outlet section and the current intensity I transported by the liquid as a function of the dimensionless flow rate Q_r for the linearly stable configurations. The diameter of the Newtonian cases is smaller than those of their viscoelastic counterparts, essentially because, as mentioned above, the shear electric stress is larger in the former case. The diameters do not scale as $Q_r^{1/2}$ in the Newtonian case [10, 37] because the jet is still accelerating at the outlet section for large flow rates. On the contrary, the current intensity transported by the Newtonian jet does follow the scaling law $I/I_o \sim Q_r^{1/2}$ [10, 37], while it considerably deviates from that prediction when small viscoelasticity is considered. The electric current convected by the viscoelastic jet is smaller than that transported by its Newtonian counterpart because the speed of the former is smaller than that of the latter.

The minimum flow rate stability limit is a very attractive parameter region of electrospray at the practical level because it leads to the continuous production of the smallest droplets while keeping a high degree of monodispersity. The effect of viscoelasticity on the minimum flow rate stability limit is shown in Fig. 8. The ratio $\lambda_r/\lambda_s = \mu^{(s)}/\mu_0$, and therefore the

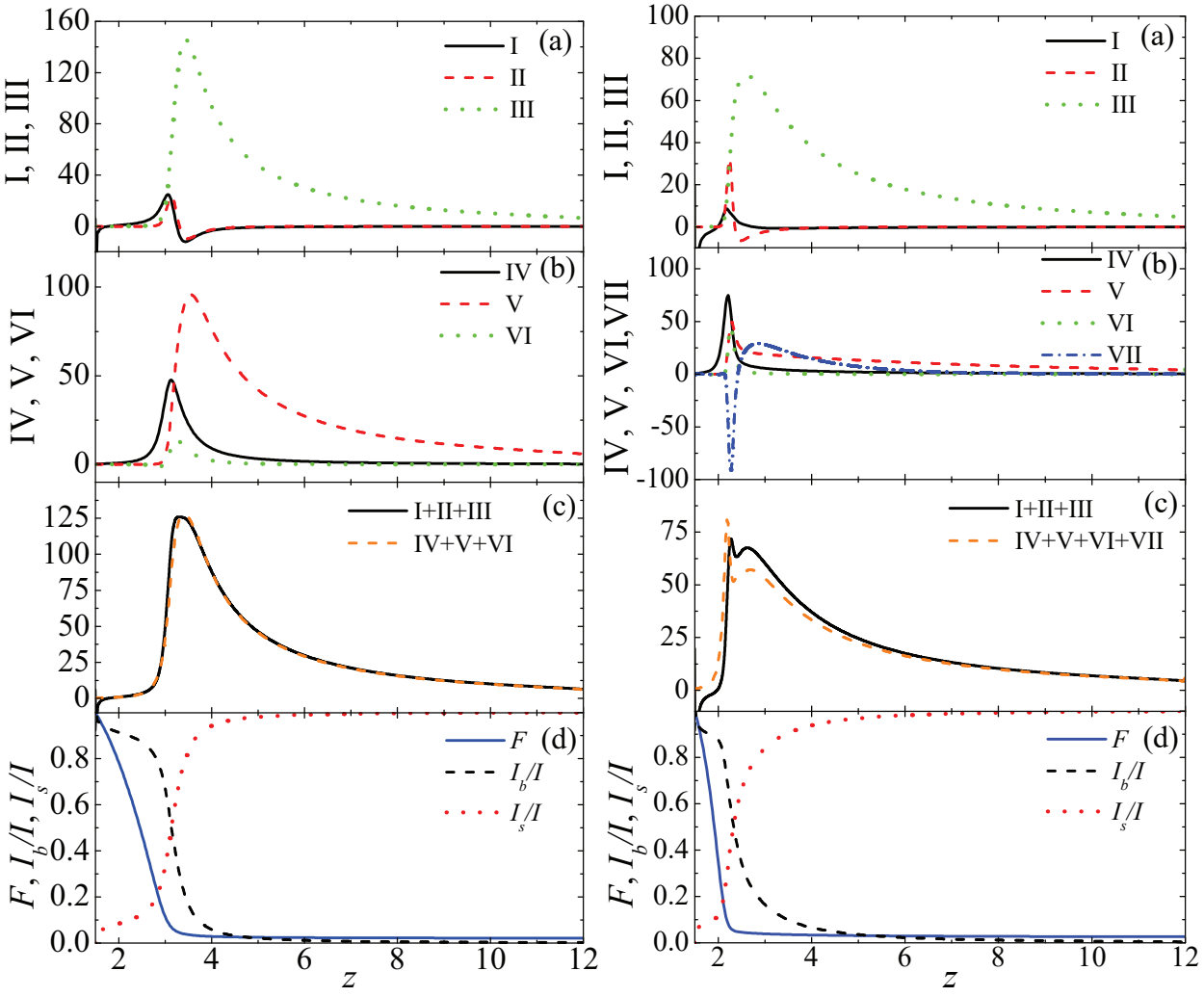

FIG. 6. (Color online) [Graphs (a), (b) and (c)] Terms I-VII of the slenderness model (24) as a function of the axial position z. [Graph (d)] Free surface position F, bulk current intensity I_b and surface current intensity I_s as a function of the axial position z. The results were calculated for $\beta = 10$, $\delta_\mu = 2.29$, $\chi = 7.92$, $Q_r = 7.72$, $\lambda_r = 0.0926\lambda_s$ and $\lambda_s = 0$ (left) and 2.656 ($\lambda_s^* = 0.108$) (right).

solution viscosity μ_0, were kept constant in all the simulations. Despite the smallness of the stress relaxation time ($\lambda_s = 0.5$ corresponds to $\widetilde{\lambda}_s = 49.2$ μs), viscoelasticity significantly reduces the minimum flow rate. This stabilizing effect can be understood in terms of the polymeric force appearing in the cone-jet transition region (Fig. 6). This force collaborates with the incipient shear electric stress in pushing the liquid throughout this critical cone-jet region, which helps the fluid to overcome the resistant forces emerging in that region. The

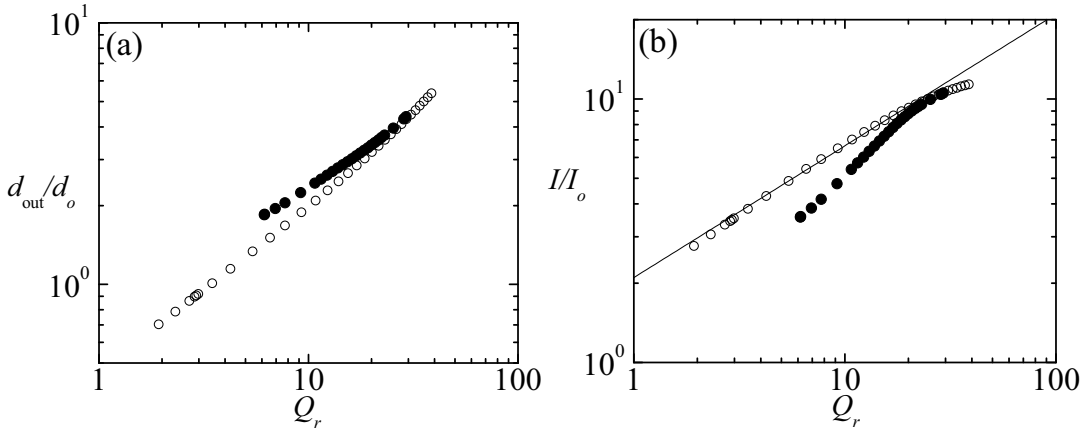

FIG. 7. Jet diameter d_{out} (a) and current intensity I (b) as a function of the dimensionless flow rate Q_r. The results were calculated for $\beta = 10$, $\delta_\mu = 2.29$, $\chi = 7.92$, $\lambda_r = 0.0926\lambda_s$ and $\lambda_s = 0$ (open symbols) and 2.656 ($\lambda_s^* = 0.108$) (solid symbols). The line in the right-hand graph is the law $I/I_o = 2.1Q_r^{1/2}$.

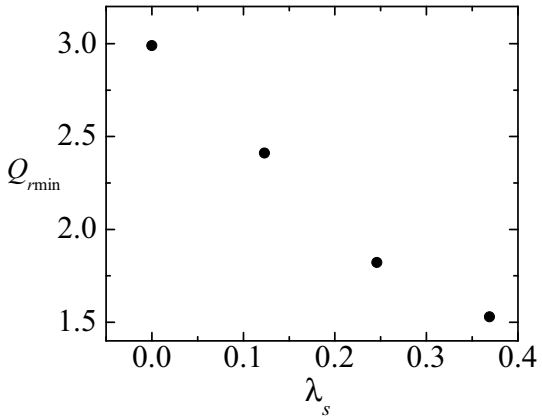

FIG. 8. Dimensionless flow rate Q_r at the minimum flow rate stability limit as a function of the stress relaxation time λ_s. The results were calculated for $\beta = 10$, $\delta_\mu = 2.29$, $\chi = 7.92$ and $\lambda_r = 0.0926\lambda_s$.

polymeric force hinders the liquid motion beyond the cone-jet transition region, where the fluid particle moves faster driven by the shear electric stress. In this sense, one may say that the liquid borrows energy from the polymeric stress in the most unstable region and returns it when safely moving downstream.

V. CONCLUSIONS

We analyzed theoretically the influence of viscoelasticity on the steady cone-jet mode of electrospray for small stress relaxation times. To this end, we numerically solved the leaky-dielectric model and calculated both the base flow and the eigenmodes characterizing its linear stability as a function of the governing parameters. We selected a well-known Newtonian electrospray realization and introduced polymeric stresses modeled by the Oldroyd-B approximation. The stress relaxation time was varied to examine the influence of those stresses on the cone-jet mode stability.

When the stress relaxation time is of the order of the residence time in the cone-jet region, fluid particles undergo an extensional deformation in that region sufficiently intense for the dissolved polymers to stretch continuously, preventing their relaxation to the coiling state. As a consequence, the axial polymeric stress becomes much larger than that produced by the solvent viscosity. This axial stress pulls from the liquid, which accelerates much faster than in the Newtonian case. This sharp acceleration makes the electrified liquid meniscus shrink. The axial polymeric stress does not play a dominant role in the final balance of energy because the kinetic energy gained by the meniscus through the action of the stretching polymers is lost in the jet region, where they eventually reach their coiling state. The meniscus shrinkage reduces the outer normal component of the electric field over the free surface, and increases the resistant force offered by both the surface tension and viscosity in the cone-jet transition region. These effects collaborate in decreasing the speed of the emitted jet with respect to that in the Newtonian case. The current intensity transported by the viscoelastic liquid is significantly smaller than that calculated in the Newtonian simulation, especially for small flow rates. The fact that the liquid gains kinetic energy from the polymeric stress in the most unstable region seems to explain the decrease of the minimum flow rate stability limit.

When a small amount of polymers is added to a Newtonian solvent, the liquid experiences two major changes: (i) polymeric stresses arise when fluid particles are deformed at sufficiently high rates, and (ii) the zero-shear viscosity increases. To analyze the effect on electrospray of the first factor exclusively, we compared numerical simulations with and without polymeric stresses for the same values of the Newtonian parameters, including the Reynolds number. The conclusions might be different from those obtained when comparing

the electrospray realizations of the solvent and the polymeric solution due to the decrease of the Reynolds number caused by the presence of the polymers.

In the present work, the conduction of electrical charges in the bulk is assumed isotropic. However, one may expect that the presence of macromolecules significantly stretched along the streamwise direction may limit the validity of that assumption in the critical cone-jet transition region. It must be noted that the inclusion of anisotropic and/or inhomogeneous conductivity in the leaky-dielectric model can violate the conservation of volumetric charge ($\nabla \cdot \mathbf{j} = 0$, $\mathbf{j}$ is the current density), which is automatically satisfied for constant scalar conductivity ($\nabla \cdot \mathbf{j} = \nabla \cdot (K\mathbf{E}) = K \nabla \cdot \mathbf{E} = 0$). In other words, the inclusion of an electrical conductivity linked to the state of the dissolved polymers at a given point may require calculating the volumetric charge density in the bulk even if the electric forces are neglected there. The molecular origin of anisotropy that renders the liquid mechanical response non-Newtonian is the same as the one that would make the ionic and thermal mobilities of species present in the liquid anisotropic: the presence of long polymeric chains highly aligned with the flow. One may argue that if non-Newtonian deviations are accounted for in the stress-strain relationship, then deviations from isotropy should be considered in the rest of properties too. However, and given the vast variety of liquid mixtures used in chemical processes and applications, there can be a large range of these mixtures that exhibit stronger mechanical deviations from isotropy than those of electrical properties, which justifies our approach; for example, the cases where ionic species are sufficiently small or electrolytes are used as solvents.

Electrospray stretches violently the fluid particles in the cone-jet transition region. As shown in this work, it can produce Deborah numbers of the order of unity when acting on viscoelastic liquids with stress relaxation times as small as hundreds of microseconds. The residence time (stretching rate) decreases (increases) with the electrical conductivity, and, therefore, one can adjust this parameter to magnify the viscoelastic character of the polymer solution. This offers the opportunity of measuring the extensional rheological properties of weakly viscoelastic liquids. For instance, it is possible (and technically simple) to measure experimentally the slenderness of the viscoelastic meniscus. Then, one can compare it with that calculated numerically as a function of the stress relaxation time to infer the value of this parameter.

Acknowledgement. This research has been supported by the Spanish Ministry of Economy, Industry and Competitiveness under Grant DPI2016-78887, and by Junta de Extremadura under Grant GR18175.

---

[1] D. H. Reneker and A. L. Yarin. Electrospinning jets and polymer nanofibers. *Polymer*, 49: 2387–2425, 2008.

[2] A. G. Kanani and S. H. Bahrami. Review on electrospun nanofibers scaffold and biomedical applications. *Trends Biomater. Artif. Organs*, 24:93–115, 2010.

[3] S. Agarwala, A. Greinera, and J. H. Wendorff. Functional materials by electrospinning of polymers. *Prog. Polym. Sci.*, 38:963–991, 2013.

[4] C. P. Carroll and Y. L. Joo. Electrospinning of viscoelastic boger fluids: Modeling and experiments. *Phys. Fluids*, 18:053102, 2006.

[5] S. Gadkari. Influence of polymer relaxation time on the electrospinning process: Numerical investigation. *Polymers*, 9:501, 2017.

[6] C. P. Carroll and Y. L. Joo. Axisymmetric instabilities of electrically driven viscoelastic jets. *J. Non-Newtonian Fluid Mech.*, 153:130–148, 2008.

[7] C. P. Carroll and Y. L. Joo. Axisymmetric instabilities in electrospinning of highly conducting, viscoelastic polymer solutions. *Phys. Fluids*, 21:103101, 2009.

[8] D. Dharmansh and P. Chokshi. Axisymmetric instability in a thinning electrified jet. *Phys. Rev E*, 93:043124, 2016.

[9] D. Dharmansh and P. Chokshi. Stability analysis of an electrospinning jet of a polymeric fluid. *Polymer*, 131:34–49, 2017.

[10] A. M. Gañán-Calvo. The surface charge in electrospraying: Its nature and its universal scaling laws. *J. Aerosol Sci.*, 30:863–872, 1999.

[11] C. Clasen, J. P. Plog, W.-M. Kulicke, M. Owens, C. Macosko, L. E. Scriven, M. Verani, and G. H. McKinley. How dilute are dilute solutions in extensional flows? *J. Rheol.*, 50:849–881, 2006.

[12] J. G. Oldroyd. On the formulation of rheological equations of state. *Proc. Roy. Soc. Lond.*, 200:523–541, 1950.

[13] R. B. Bird, R. C. Armstrong, and O. Hassager. *Dynamics of Polymeric Liquids*. John Wiley

& Sons, Inc., United States of America, 1987.

[14] P. P. Bhat, S. Appathurai, M. T. Harris, M. Pasquali, G. H. McKinley, and O. A. Basaran. Formation of beads-on-a-string structures during break-up of viscoelastic filaments. *Nat. Phys*, 6:625–631, 2010.

[15] M. S. N. Oliveira and G. H. McKinley. Iterated stretching and multiple beads-on-a-string phenomena in dilute solutions of highly-extensible flexible polymers. *Phys. Fluids*, 17:071704, 2005.

[16] C. Clasen, J. Eggers, M. A. Fontelos, J. Li, and G. H. McKinley. The beads-on-string structure of viscoelastic threads. *J. Fluid Mech.*, 556:283–308, 2006.

[17] J. R. Melcher and G. I. Taylor. Electrohydrodynamics: a review of the role of interfacial shear stresses. *Annu. Rev. Fluid Mech.*, 1:111–146, 1969.

[18] D. A. Saville. Electrohydrodynamics: The Taylor-Melcher leaky dielectric model. *Annu. Rev. Fluid Mech.*, 29:27–64, 1997.

[19] F. J. Higuera. Numerical computation of the domain of operation of an electrospray of a very viscous liquid. *J. Fluid Mech.*, 648:35–52, 2010.

[20] M. A. Herrada, J. M. López-Herrera, A. M. Gañán-Calvo, E. J. Vega, J. M. Montanero, and S. Popinet. Numerical simulation of electrospray in the cone-jet mode. *Phys. Rev. E*, 86: 026305, 2012.

[21] A. Ponce-Torres, N. Rebollo-Muñoz, M. A. Herrada, A. M. Gañán-Calvo, and J. M. Montanero. The steady cone-jet mode of electrospraying close to the minimum volume stability limit. *J. Fluid Mech.*, 857:142–172, 2018.

[22] M. Gamero-Castaño and M. Magnani. Numerical simulation of electrospraying in the cone-jet mode. *J. Fluid Mech.*, 859:247–267, 2019.

[23] V. Theofilis. Global linear instability. *Annu. Rev. Fluid Mech.*, 43:319–352, 2011.

[24] P. J. Schmid. Nonmodal stability theory. *Annu. Rev. Fluid Mech.*, 39:129–162, 2007.

[25] F. Cruz-Mazo, M. A. Herrada, A. M. Gañán-Calvo, and J. M. Montanero. Global stability of axisymmetric flow focusing. *J. Fluid Mech.*, 832:329–344, 2017.

[26] G. I. Barenblatt. *Scaling*. Cambridge University Press, Cambridge, UK, 2003.

[27] A. M. Gañán-Calvo, N. Rebollo-Muñoz, and J. M. Montanero. Physical symmetries and scaling laws for the minimum or natural rate of flow and droplet size ejected by taylor cone-jets. *New J. Phys.*, 15:033035, 2013.

[28] W. J. Scheideler and C.-H. Chena. The minimum flow rate scaling of taylor cone-jets issued from a nozzle. *Appl. Phys. Lett.*, 104:024103, 2014.

[29] J. Carlier, S. Arscott, J-C. Camart, C. Cren-Olivé, and S. Le Gac. Integrated microfabricated systems including a purification module and an on-chip nano electrospray ionization interface for biological analysis. *J. Chromatogr. A*, 1071:213–22, 2005.

[30] E. M. Yuill, N. Saand S. J. Ray, G. M. Hieftje, and L. A. Baker. Electrospray ionization from nanopipette emitters with tip diameters of less than 100 nm. *Anal. Chem.*, 85:8498–8502, 2013.

[31] D. F. James. Boger fluids. *Annu. Rev. Fluid Mech.*, 41:129–142, 2009.

[32] T. Funada and D.D. Joseph. Viscoelastic potential flow analysis of capillary instability. *J. Non-Newtonian Fluid Mech*, 111:87–105, 2003.

[33] A. M. Gañán-Calvo, J. C. Lasheras, J. Dávila, and A. Barrero. The electrostatic spray emitted from an electrified conical meniscus. *J. Aerosol Sci.*, 25:1121–1142, 1994.

[34] M. A. Herrada and J. M. Montanero. A numerical method to study the dynamics of capillary fluid systems. *J. Comput. Phys.*, 306:137–147, 2016.

[35] P. C. Sousa, E. J. Vega, R. G. Sousa, J. M. Montanero, and M. A. Alves. Measurement of relaxation times in extensional flow of weakly viscoelastic polymer solutions. *Rheol. Acta*, 56: 11–20, 2017.

[36] E. Turkoz, J. M. López-Herrera, J. Eggers, C. B. Arnold, and L. Deike. Axisymmetric simulation of viscoelastic filament thinning with the olroyd-b model. *J. Fluid Mech.*, 851:R2, 2018.

[37] A. M. Gañán-Calvo, J. M. López-Herrera, M. A. Herrada, A. Ramos, and J. M. Montanero. Review on the physics electrospray: from electrokinetics to the operating conditions of single and coaxial Taylor cone-jets, and AC electrospray. *J. Aerosol Sci.*, 125:32–56, 2018.